Vibration Suppression Using Single Neuron-Based PI Fuzzy Controller and Fractional-Order Disturbance Observer

Wen Li and Yoichi Hori, *Fellow, IEEE*

***Abstract*—An approach is proposed for vibration suppression in a two-inertia system using an integration of a fractional-order disturbance observer and a single neuron-based PI fuzzy controller. The former is used to obtain disturbance estimate and generate compensation signal, and the latter is utilized to realize outer loop control. Fractional-order disturbance observer has a wider range to select a suitable tradeoff between robustness and vibration suppression, because introduction of fractional calculus makes universe of relative degree of Q-filter is expanded from integer domain to real-number domain. For the single neuron-based PI fuzzy controller, a single neuron makes up a PI controller and such a controller is embedded in each cell of the fuzzy control table. Thus, the fuzzy control table is changed into a controller matrix and it constructs a nonlinear adaptive controller with parameter self-tuning property. Experimental results illustrate that the integration of fractional-order disturbance observer and single neuron-based PI fuzzy controller can improve the performance of disturbance attenuation and system robustness.**

***Index Terms*—Fuzzy neural controller, fractional-order observer, vibration suppression.**

I. Introduction

VIBRATION, the repetitive motion of objects relative to a stationary frame of reference or nominal position, occurs in most machines, structures, and dynamic systems. Vibration can be found in daily life, as well as in engineering, which causes noise, reduces accuracy, and reliability of equipments. Thus, vibration suppression and disturbance rejection is an important problem.

It is well known that, in practice, a physical motion control system will not be exactly the same as any mathematical model, no matter how the model is obtained. Although all models cannot describe practice systems precisely, some of them might be useful. Disturbance observers (DOBs) just use the difference between the actual output and the output of the nominal model to compensate the output of the controller. In the absence of large modeling errors, DOBs are able to improve disturbance rejection characteristics and command following characteristics. The filter in DOB usually is a low-pass filter, called Q-filter. There are three parameters, order, relative degree, and the bandwidth of Q-filter. Thus, comparing with integral action, DOB has more flexibility[1], [2]. Although by appending disturbance states to a traditional state estimator, the disturbance compensation can be realized, using the disturbance observer structure allows simple and intuitive tuning of disturbance observer loop gains independent of the state feedback gains [3]. It is the reason why to use disturbance observer is a more common practice in many high precision motion control systems [4].

It is well known that an industrial servo system generally is a multi-inertia system with several inertia moments and springs, and it can be analyzed by an approximate two-inertia system. This two-inertia system can be seen as a simplest vibration model of typical mechatronic system. Thus, in this paper, the problem of vibration suppression in the two-inertia system is discussed. Because a torque transmission system is composed of several gears and couplings, it is flexible. For such a system, the torsion vibration occurs when the motor speed abruptly changes. In order to improve response and accuracy of the system, there are many contributions to the study of vibration suppression of the two-inertia system. More usual methods are typically simulator following control [5], speed differential feedback control [6], disturbance observer-based control [7], [8], and state feedback control [9], [10], etc. Several disturbance observer-based approaches were investigated and simulated with Matlab/Simulink to find out a suitable solution for the industrial application in [11] for the main drive system of cycloconverter-fed 1450 rolling mill in a steel works. Recently, applications of fractional calculus theory in practical control field have increased significantly, e.g., the fractional-order disturbance observer (FO-DOB) was proposed [12], in order to solve the tradeoff between the phase margin loss and the strength of the low-frequency vibration suppression for a traditional DOB [12].

In order to make the system have better robust stability against variation of mechanical parameters and obtain a desired steady-state precision, this paper presents an approach for vibration suppression in the two-inertia system using a combination of a FO-DOB and a single neuron-based PI fuzzy controller (NPIFC). A FO-DOB and a NPIFC establish an active vibration suspension unit in the two-inertia torsional experimental system. The FO-DOB is used to estimate disturbance and to generate compensation signal, and the NPIFC is used to realize outer loop control. Three parts are contained in this paper. In first part, the two-inertia torsional experimental system used for

Manuscript received July 5, 2005; revised December 15, 2005. Abstract published on the Internet November 30, 2006. This paper was supported in part by the China Scholarship Council and Science and Technology Fund of the Ministry of Education P.R.C.

W. Li is with the Department of Electrical Engineering, Dalian JiaoTong University, Dalian, Liaoning Province 116028, China (e-mail: lw6017@vip.sina.com).

Y. Hori is with the Information Electronics Division, Electrical Control System Engineering, Institute of Industrial Science, University of Tokyo, Tokyo 153-8505, Japan (e-mail: hori@iis.u-tokyo.ac.jp; y.hori@ieee.org).

Color versions of one or more of the figures in this paper are available online at http://ieeexplore.ieee.org.

Digital Object Identifier 10.1109/TIE.2006.888771

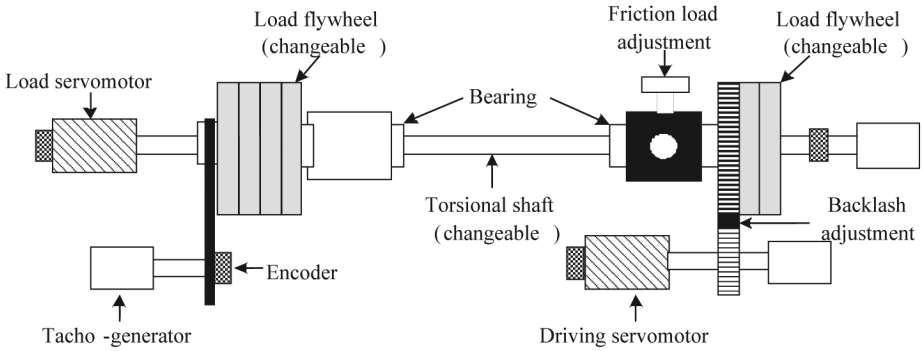

Fig. 1. Torsional experimental system.

the research of vibration suppression is introduced first. Then, the relation between robustness and parameters of $Q(s)$-filter is discussed by giving an instance of continuous-time disturbance observer. Next, it is analyzed why FO-DOB has more flexibility than DOB for vibration suppression. Finally, the FO-DOB design of the two-inertia torsional experimental system is given. The second part of this paper gives the design idea, structure, and design method of NPIFC. The basic framework of NPIFC is a control table-based fuzzy controller. It has fast real-time property and better robust stability. However, it is difficult to get good steady-state precision. To improve steady-state precision, a PI controller realized by a single neuron is embedded in each cell of the control table, it is called NPI for short. Because of the introduction of neurons, the fuzzy control table has learning property. Because the control table is transformed into a PI controller matrix, the fuzzy controller is actually changed into a nonlinear adaptive controller. Specific design steps of NPIFC are given in this part later. The third part shows some experiments of FO-DOB robustness in such cases of different backlash. The comparison experiments of different controllers also are presented to illustrate the validity of the proposed vibration suppression approach in a two-inertia system. Finally, some conclusions are given.

II. Fractional-Order Disturbance Observer Design

A. Mathematical Model of the Two-Inertia Torsional Experiment System

Before discussing disturbance observer, a torsional experimental system used for the research of vibration suppression is introduced first. The system is depicted in Fig. 1, which illustrates a typical configuration of an industrial servo system. Corresponding to the experimental system shown in Fig. 1, a simplified two-inertia model can be drawn, as shown in Fig. 2. From Fig. 1, it can be found that two flywheels of the system are connected with a long and thin torsional shaft, and the connection between driving shaft and slave shaft by a pair of gears with gear ratio 2:1. Therefore, the torsion vibration will occur because of torsional elasticity of shaft and imperfect rigidity of gears when torque is transmitted. A block diagram of the two-inertial model is given in Fig. 3 and parameters of the two-inertia model are listed in Table I. In addition, the backlash between two gears can be adjusted and an additional friction can be put on the shaft.

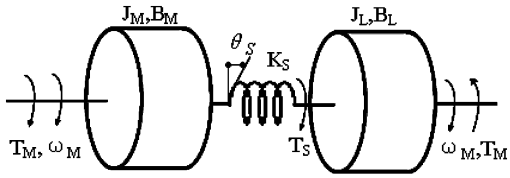

Fig. 2. Simplified two-inertia model.

According to Fig. 3, without considering the backlash, the transfer function from input torque T_M to driving motor angular speed ω_m, can be derived, as shown in (1) at the bottom of the page. When the viscous friction in the two-inertia model are neglected, i.e., B_M and B_L are zero, (1) will become

$$G_{pM2}(s) = \frac{\omega_M(s)}{T_M(s)} = \frac{s^2 + \omega_a^2}{J_M s(s^2 + \omega_0^2)} \tag{2}$$

where resonant frequency

$$\omega_0 = \sqrt{K_S\left(\frac{1}{J_M} + \frac{1}{J_L}\right)} = 317.55\ \left(\frac{\text{rad}}{\text{sec}}\right) \tag{3}$$

antiresonant frequency

$$\omega_a = \sqrt{\frac{K_S}{J_L}} = 226.57\ \left(\frac{\text{rad}}{\text{sec}}\right). \tag{4}$$

$$G_{pM1}(s) = \frac{\omega_M(s)}{T_M(s)} = \frac{J_L s^2 + B_L s + K_S}{J_M J_L s^3 + (J_M B_L + J_L B_M)s^2 + [K_S(J_M + J_L) + B_M B_L]s + K_S(B_M + B_L)} \tag{1}$$

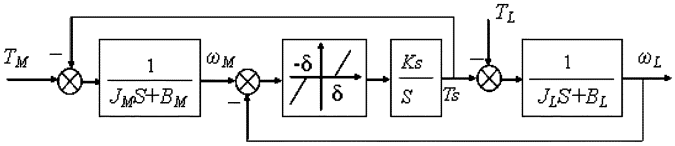

Fig. 3. Block diagram of the two-inertial model.

TABLE I
PARAMETERS OF THE TWO-INERTIA MODEL

J_M	The equivalent inertia of driving side: $4.01558\times10^{-3}\ (Kg\cdot m^2)$
J_L	The equivalent inertia of load side: $3.8674\times10^{-3}\ (Kg\cdot m^2)$
K_S	Shaft torsional elastic coefficient: 198.5 (Nm/rad)
T_M	The torque of driving motor
T_L	Disturbance torque
ω_M	The angular speed of driving motor
ω_L	Load angular speed
δ	Backlash

Rearranging the following expression:

$$\omega_0 = \sqrt{\frac{K_S}{J_L}\left(1+\frac{J_L}{J_M}\right)} = \omega_a\sqrt{1+\frac{J_L}{J_M}}$$

and let

$$H_0 = \frac{\omega_0}{\omega_a}\sqrt{1+R_0} \text{ and } R_0 = \frac{J_L}{J_M} \tag{5}$$

where H_0 and R_0 are called resonance ratio and the inertia ratio, respectively. H_0 and R_0 are important parameters in the system [13]. The Bode curves of the transfer function described by (1) with different viscous friction coefficients are given in Fig. 4.

B. Continuous-Time Disturbance Observer Analysis

This section discusses the basic mechanism of disturbance observer and relations between robustness and parameters of $Q(s)$-filter.

In order to realize disturbance suppression, the basic idea of disturbance observer is to use a nominal model of the plant to estimate the disturbance caused by outer interference torque and parameter variation, and an equivalent compensation action is generated from the estimate. A basic architecture of conventional disturbance observer is shown in Fig. 5, where $G_p(s)$ is plant transfer function, d is equivalent disturbance, $\tilde{d}_f$ is the observing value (estimate) of d, and c is the output of the outer loop controller. The estimate of equivalent disturbance can be calculated from Fig. 5 by

$$\tilde{d}_f = (u+d)G_p(s)G_p^{-1}(s) - u = d. \tag{6}$$

However, three problems are encountered for this disturbance observer in a practice physical system [14] as follows.

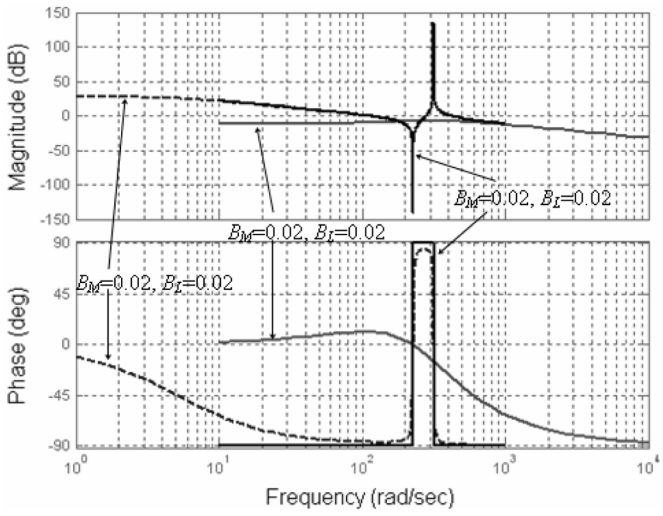

Fig. 4. Bode curve of different B_M and B_L.

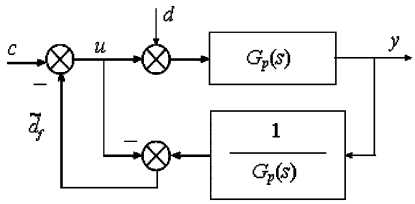

Fig. 5. Basic architecture of DOB.

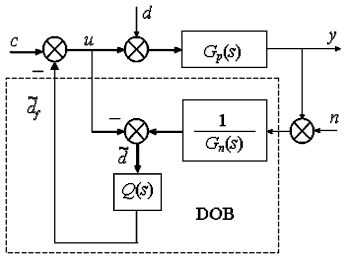

Fig. 6. Block diagram of DOB.

1) In a usual case, the relative order of $G_p(s)$ is not equal to zero, so that the inverse cannot be realized physically.
2) It is difficult to built an accurate plant model, $G_p(s)$.
3) If measurement noise is considered, control performance will be deteriorated.

A $Q(s)$-filter and a nominal model $G_n(s)$ instead of $G_p(s)$ are introduced to solve the above problems also shown as Fig. 6. Fig. 6 is a conventional disturbance observer, where y and n are the output and noise, respectively. Usually, the $Q(s)$-filter is a low-pass filter to restrict the effective bandwidth of the DOB. Signals $\tilde{d}$ and $\tilde{d}_f$ are the disturbance estimate before and after filtering by the $Q(s)$-filter. The following three expressions are derived from Fig. 6:

$$G_{cy}(s) = \frac{Y(s)}{C(s)} = \frac{G_p(s)G_n(s)}{G_n(s)+Q(s)(G_p(s)-G_n(s))} \tag{7}$$

$$G_{dy}(s) = \frac{Y(s)}{D(s)} = \frac{{}_p(s)G_n(s)(1-Q(s))}{G_n(s)+Q(s)(G_p(s)-G_n(s))} \tag{8}$$

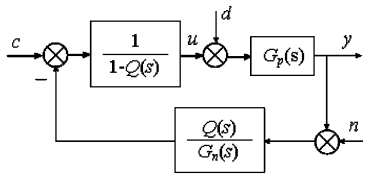

Fig. 7. Equivalent block diagram of DOB.

$$G_{ny}(s) = \frac{Y(s)}{N(s)} = \frac{G_p(s)Q(s)}{G_n(s) + Q(s)(G_p(s) - G_n(s))}. \quad (9)$$

Suppose the cutoff frequency of low-pass $Q(s)$-filter is ω_q, then when $\omega \ll \omega_q$, $Q(s) \approx 1$, there are relations $G_{cy}(s) \approx G_n(s)$, $G_{dy}(s) \approx 0$, and $G_{ny}(s) \approx 1$; and when $\omega \gg \omega_q$, $Q(s) \approx 0$, there are relations $G_{cy}(s) \approx G_p(s)$, $G_{dy}(s) \approx G_p(s)$, and $G_{ny}(s) \approx 0$. From these relations, it can be found that the outer disturbance can be suppressed by designing a low-pass $Q(s)$-filter design. That is to say, the design of $Q(s)$-filter is an important step in DOB design. First, the number of relative orders of the $Q(s)$-filter should not be less than that of $G_n(s)$ to maintain $Q(s)G_n^{-1}(s)$ being a regular rational transfer function, and then the selection of bandwidth should be a compromise between robust stability and disturbance suppressing force of DOB.

The relation between real-model $G_p(s)$ and nominal model $G_n(s)$ may be expressed by

$$G_p(s) = G_n(s)(1 + \Delta(s)) \quad (10)$$

where $\Delta(s)$ is a variable transfer function, which describes uncertainty of the plant. According to the theorem of robust stability, the sufficiency criterion of robust stability for $Q(s)$ [14] is

$$\|\Delta(s)Q(s)\|_\infty \leq 1. \quad (11)$$

Equation (11) is a foundation of designing $Q(s)$.

In order to analyze the relation between robustness and frequency bandwidth (described by ω_q) of $Q(s)$-filter, an equivalent block diagram of the DOB, as shown in Fig. 6, is given in Fig. 7.

To simplify the analysis, assume that e^{-sT_d} is the only source of unmodeled dynamics, that is

$$G_p(s) = G_n(s)e^{-sT_d}. \quad (12)$$

From (10) and (12), the variable transfer function can be expressed as follows:

$$\Delta(s) = e^{-sTd} - 1. \quad (13)$$

Furthermore, from the $1/1 - Q(s)$ block in Fig. 7, it is shown clearly that the disturbance observer is a high gain technique as $Q(s) \to 1$ is a low-frequency domain. However, the unmodeled dynamics limits the allowable loop gain to assure the robustness. The variations of robust stability with respect to ω_q and relative degree n_q of $Q(s)$-filter are illustrated in Figs. 8 and 9,

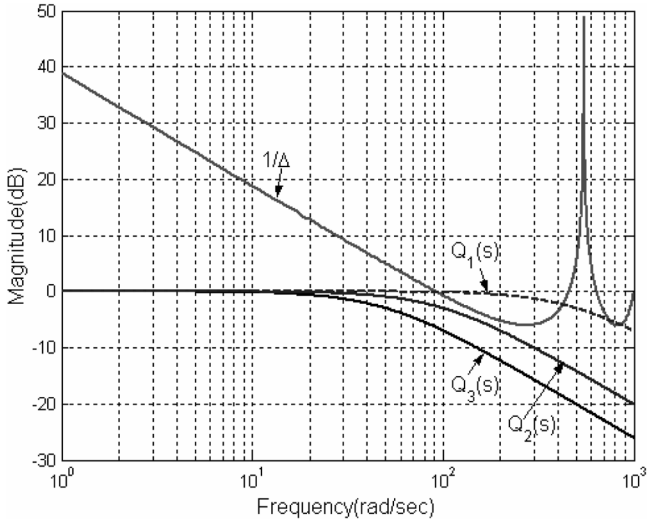

Fig. 8. Q-filter bandwidth limitation.

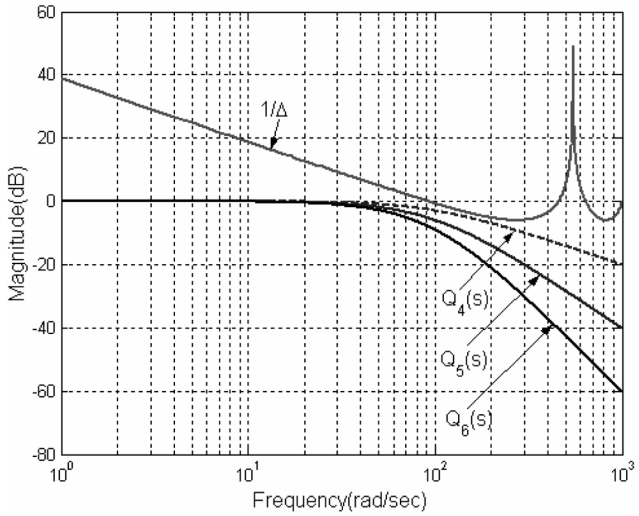

Fig. 9. The effect of n_q in DOB.

respectively. Suppose low-pass $Q(s)$-filters have the following form:

$$Q(s) = \frac{1}{(\tau s + 1)^{n_q}} \quad (14)$$

where $\omega_q = 1/\tau$. Three $Q(s)$-filters, $Q_1(s)$, $Q_2(s)$, and $Q_3(s)$ are considered and their cutoff frequencies are 500, 100, and 50. Here, the value $T_d = 0.2$ ms is used in (13).

Fig. 8 illustrates that, when the cutoff frequency is 500 rad/s, the robust stability criteria of (11) is clearly violated; for the 100 rad/s case, the magnitude response of filter $Q_2(s)$ is close to, but remains below the curve of $1/\Delta$. Since other sources of model error invariably exist in a real system and still the gain of outer loop feedback compensation should be considered, the cutoff frequency ω_q of $Q(s)$-filter should not be more than 100 rad/s. Fig. 9 shows three curves, $Q_4(s)$, $Q_5(s)$, and $Q_6(s)$ with different relative degrees, $n_q = 1,2,3$, and the same cutoff frequency of 100 rad/s. Fig. 9 also shows that the higher the relative degree n_q of $Q(s)$-filter, the better the robust stability for a fixed ω_q. Literature [3] and [12] discuss the issue of the loss of

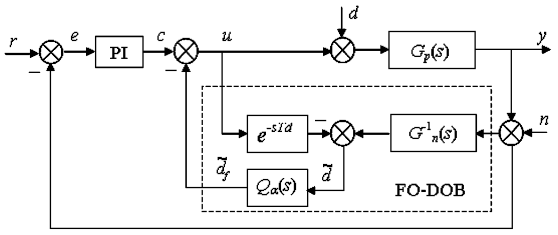

Fig. 10. Block diagram of FO-DOB in a system.

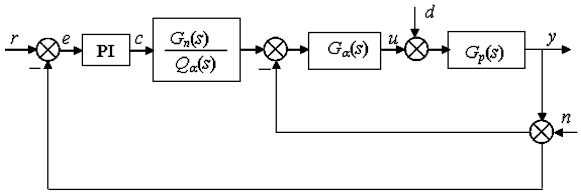

Fig. 11. An equivalent block diagram of Fig. 10.

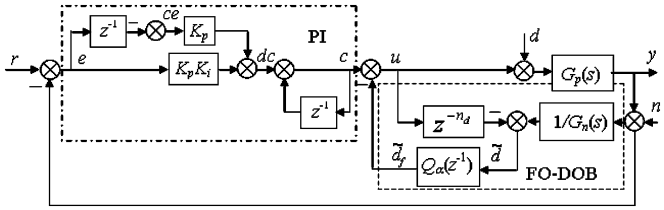

Fig. 12. Digital realization of system.

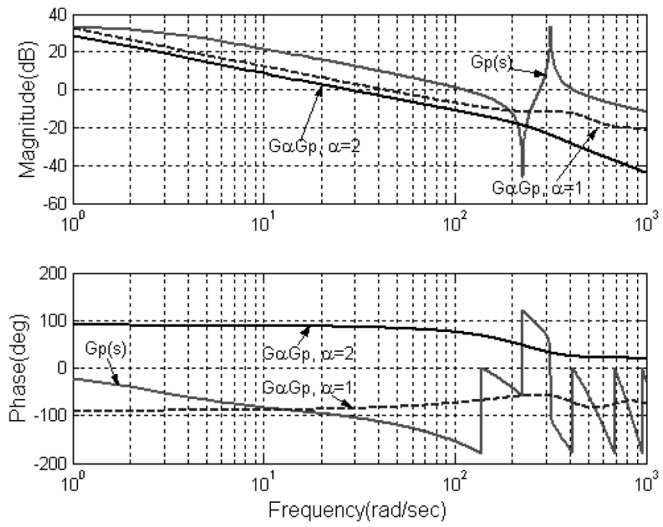

Fig. 13. Bode curve with $Td = 0.2$ ms.

phase margin with DOB in details, and give a figure ([3, Fig. 6]) to guide the right selection of ω_q and n_q. However, ω_q usually is determined according to the disturbance attenuation requirement in advance. In fact, n_q is the only knob to tune the tradeoff. Consequently, if n_q can be selected in real-number domain R instead of integer domain I, the selecting range will be increased greatly. When n_q belongs to R, accordingly, the disturbance observer is a FO-DOB.

C. Fractional-Order Disturbance Observer Design

From the above analysis, it can be clearly seen that FO-DOB has more flexibility than DOB for disturbance rejection, just because relative degree n_q of Q-filter in FO-DOB can be selected in a real-number domain instead of the original integer domain. Here, n_q is denoted by $\alpha \in R$ and Q-filter has become a fractional-order filter, denoted by $Q_\alpha(s)$. In other words, α can be continuously tuned to select a suitable tradeoff between robust stability and disturbance attenuation.

Figs. 10 and 11 show the block diagram of a FO-DOB in a system and its equivalent block diagram. A FO-DOB is usually realized in the form of digital type. Fig. 12 is the digital implementation. Figs. 11 and 12 are the equivalent block diagram and the digital form of Fig. 10, respectively, where $G_\alpha(s)$ is called as equivalent compensator; $G_n(z^{-1})$ is the discrete form of nominal model $G_n(s)$; $Q_\alpha(z^{-1})$ is the discrete expression of $Q_\alpha(s)$; and n_d is the number of pure time delay steps of the control signal u. In fact, it is an estimate of pure delay steps n_p of $G_p(z^{-1})$ [4].

Next, is an analysis about equivalent compensator $G_\alpha(s)$. The expression of $G_\alpha(s)$ can be derived from Figs. 10 and 11

$$G_\alpha(s) = \frac{Q_\alpha(s)}{1 - Q_\alpha(s)e^{-sT_d}} G_n^{-1}(s). \tag{15}$$

From (1), a nominal model can be descried by

$$G_n(s) = \frac{b_2 s^2 + b_1 s + b_0}{s^3 + a_2 s^2 + a_1 s + a_0} \tag{16}$$

and (14) is rewritten as

$$Q_\alpha(s) = \frac{1}{(\tau s + 1)^\alpha}. \tag{17}$$

As previously mentioned, the relative degree α should not be less than 1 to keep $Q_\alpha(s)G_n^{-1}(s)$ regular.

From (12) and (15)–(17), it can be seen that $G_\alpha(s)$ is a fractional-order transfer function and its numerator is equal to the denominator of $G_p(s)$. It is propitious to reject the low-frequency vibration. Figs. 13 and 14 show Bode curves of $G_p(s)$, $G_{\alpha=1}(s)G_p(s)$, and $G_{\alpha=2}(s)G_p(s)$ when $Td = 0.2$ ms and $Td = 0$ ms, respectively. The low-frequency vibration suppression action of equivalent compensator in inner loop can be seen from them clearly. Also, it can be found that time delay causes high-frequency performance to be worse, but if increasing α, the affect will be weakened. By using FO-DOB, a rational tradeoff among the strength of low-frequency vibration suppression, robust stability, and high-frequency property can be made easier than by using DOB, because α can be tuned in real-number domain continuously.

According to the above analysis, parameters of the FO-DOB are selected for the two-inernial torsional experimental system, frequency bandwidth $\omega_q = 100$ rad/s, α as in [1] and [2]. One of the realization methods of fractional-order $Q_\alpha(s)$-filter is to

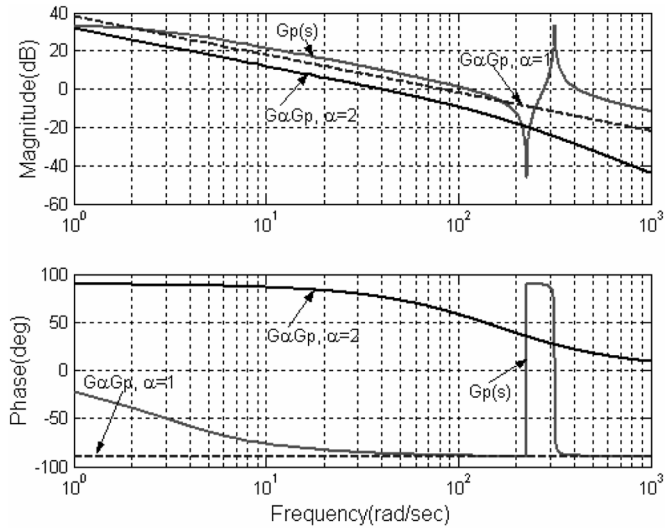

Fig. 14. Bode curve with $Td = 0$ ms.

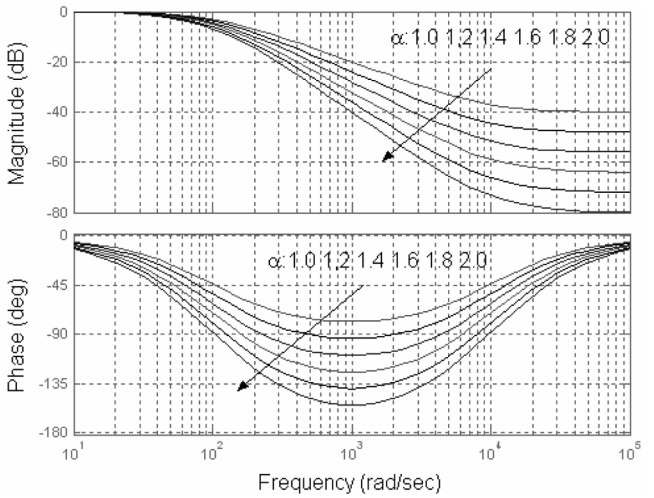

Fig. 15. Bode curves of $Q_\alpha(s)$ with different α.

use a continuous integer-order filter $D_N(s)$ in a selected frequency bandwidth $[\omega_b, \omega_h]$ to approximate the fractional-order $Q_\alpha(s)$-filter [15]. General form of $D_N(s)$ is given as follows:

$$D_N(s) = K \prod_{k=-N}^{N} \frac{s+\omega_k}{s+\omega_k}. \tag{18}$$

Mechanism and steps of this approximation method are explained in [15]. Bode curves of $Q_\alpha(s)$-filter with different α, $N = 2$, and approximation bandwidth [100,10000], are depicted in Fig. 15. Here, $Q_\alpha(s)$-filter is approximated by a five-order filter $D_{N=2}(s)$. That is

$$Q_\alpha(s) \approx \frac{b_5 s^5 + b_4 s^4 + b_3 s^3 + b_2 s^2 + b_1 s + b_0}{a_5 s^5 + a_4 s^4 + a_3 s^3 + a_2 s^2 + a_1 s + a_0}. \tag{19}$$

Equation (20) is an example when $\alpha = 1.6$, as shown in (20) at the bottom of the page.

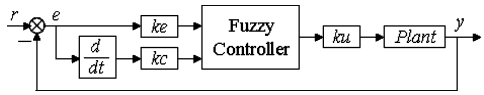

Fig. 16. FC for two-inertial system.

TABLE II
FUZZY CONTROL RULE TABLE $U\ (E, CE)$

Ei \ Cj		1	2	3	4	5	6	7
		NL	NM	NS	ZE	PS	PM	PL
1	NL	1	1	1	2	2	3	3
2	NM	1	1	2	3	3	4	4
3	NS	1	2	2	3	4	5	5
4	ZE	2	3	4	4	4	5	6
5	PS	3	3	4	5	6	6	7
6	PM	4	4	5	5	6	7	7
7	PL	5	5	6	6	7	7	7

III. DESIGN OF SINGLE NEURON-BASED PI FUZZY CONTROLLER

In order to provide an appropriate control input strength, to enhance the robust stability against variation of mechanical parameters and to obtain a desired steady precision, a NPIFC is proposed in this section. The basic framework of this controller is a fuzzy controller (FC) based on the control table, and it is put in the outer loop. Because of the control table-based FC, the input–output space of the system is divided into several partitions by the control table. In order to improve the control precision and to introduce the learning function for the FC, a PI controller constructed by a single neuron is embedded in each cell of the control table. Therefore, the fuzzy control table becomes a matrix of PI controllers with self-tuning parameter performance. This matrix constructs a nonlinear adaptive controller.

A. Introduction of Classical Fuzzy Controller (FC)

Generally speaking, there are three steps for designing a simple FC, as shown in Fig. 16: 1) choosing appropriate input, output variables, and defining them; 2) defining linguistic variables to form a data base; and 3) establishing a control rule

$$Q_{1.6}(s) \approx \frac{s^5 + 2.168\times10^4 s^4 + 1.318\times10^8 s^3 + 2.754\times10^{11} s^2 + 1.977\times10^{14} s + 3.981\times10^{16}}{1585 s^5 + 7.873\times10^6 s^4 + 1.096\times10^{10} s^3 + 5.248\times10^{12} s^2 + 8.632\times10^{14} s + 3.981\times10^{16}} \tag{20}$$

TABLE III
FUZZY CONTROL TABLE

CE / E	-6	-5	-4	-3	-2	-1	0	1	2	3	4	5	6
-6	-5.17	-5.09	-5.04	-4.68	-4.53	-4.00	-3.63	-3.53	-3.14	-2.40	-1.68	-1.39	-1.43
-5	-5.09	-5.09	-4.95	-4.46	-4.17	-3.44	-3.02	-2.95	-2.65	-1.88	-1.21	-0.97	-0.97
-4	-5.04	-4.95	-5.04	-4.46	-3.90	-3.17	-2.41	-2.33	-1.95	-1.52	-0.72	-0.46	-0.44
-3	-4.68	-4.46	-4.46	-4.46	-3.74	-3.00	-2.05	-1.33	-0.86	-0.25	0.25	0.60	0.60
-2	-4.53	-4.17	-3.58	-3.37	-3.43	-2.80	-2.02	-0.87	0.00	0.86	1.38	1.66	1.68
-1	-4.00	-3.44	-2.95	-2.32	-2.26	**-2.24**	**-1.66**	**-0.87**	0.17	1.33	2.33	2.76	2.76
0	-3.41	-3.02	-2.41	-1.78	-1.13	**-0.85**	**0.00**	**0.85**	1.13	1.78	2.41	3.02	3.41
1	-2.76	-2.76	-2.33	-1.33	-0.17	**0.87**	**1.66**	**2.24**	2.26	2.32	2.95	3.44	4.00
2	-1.68	-1.66	-1.38	-0.86	0.00	0.87	2.02	2.80	3.43	3.37	3.58	4.17	4.53
3	-0.60	-0.60	-0.25	0.25	0.86	1.33	2.05	3.00	3.74	4.46	4.46	4.46	4.68
4	0.44	0.46	0.72	1.52	1.95	2.33	2.41	3.17	3.90	4.46	5.04	4.95	5.04
5	0.97	0.97	1.21	1.88	2.65	2.95	3.02	3.44	4.17	4.46	4.95	5.09	5.09
6	1.43	1.39	1.68	2.40	3.14	3.53	3.63	4.00	4.53	4.68	5.04	5.09	5.17

base. In this paper, the error of driver angular speed ω_d denoted by e and its change-in-error denoted by ce are taken as input variables of the FC, the control torque T_m of the driver is the output variable. Corresponding fuzzy variables are denoted by E, CE, and U, respectively, and each has seven linguistic values. Table II is the control rule table designed for the two-inertial torsional experimental system. For convenience, triangular and trapezoidal functions are used as membership functions for inputs and output. When using singleton fuzzification and Zadeh's compositional rule of inference, which uses the *max/min* operators, the fuzzy control table can be acquired by offline calculation, as shown in Table III.

Scaling gains, k_e, k_c, and k_u, play an important role on the effect of system response. Here, the changing range of error is $(-e_m, e_m)$, and the changing range of change-in-error is $(-ce_m, ce_m)$. Applying formula (21), the two universes of discourse can be transformed into the range $[-6, 6]$ considered in FC

$$y = \frac{12}{x_b - x_a}\left(x - \frac{x_a + x_b}{2}\right). \tag{21}$$

Substituting x_a, x_b with $-e_m$, e_m and $-ce_m$, ce_m, respectively, the input scaling gains $k_e = 6/e_m$, $k_c = 6/ce_m$ can be obtained easily. The process of getting $k_u = u_m/6$ is the opposite process of getting k_e and k_c because control output should be transformed from fuzzy universe [-6, 6] to crisp universe $[-u_m, u_m]$. e_m, ce_m and u_m should be decided according to system parameters and control requirement. For the two-inertial torsional experimental system, $e_m = \kappa\omega_{d\_\mathrm{ref}}$, $\kappa \le 1$ (setting angular speed of driver), $ce_m = \lambda\omega_{d\_\mathrm{ref}}$, $\lambda \le 1$, $u_m = \gamma \ \mathrm{tor}\ q_{\max}$, $\gamma \le 1$ ($\mathrm{tor}\ q_{\max}$ is the maximum torque value of driver). These scaling gains can be tuned by selecting different κ, λ, γ. The tuning of scaling gains for fuzzy systems is often referred to as scaling a fuzzy system. In fact, the tuning results in the effect of contracting or spreading membership functions of input or output. Fig. 17 shows the control surface of this FC.

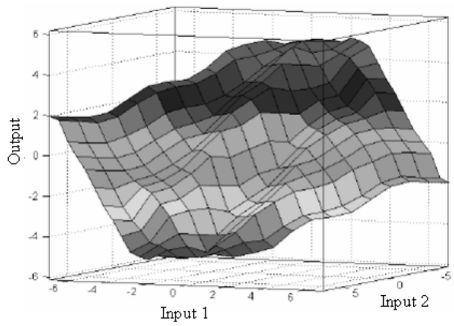

Fig. 17. Control surface of FC.

B. NPIFC Design

It is well-known that fuzzy systems have lower sensitivity for parameter change and satisfy the "universal approximation property" [16]. In other words, fuzzy systems actually have very strong functional capabilities. That is, if properly constructed, they can perform very complex operations. However, fuzzy systems also lack the following, such as no learning ability and lower precision of steady-state. Therefore, a NPIFC is proposed, it is the main contribution of this paper. Construction of this NPIFC is based on the following consideration.

1) Introduce a single neuron into each cell of the control table to make the FC have a learning function.
2) Construct a PI controller using a single neuron in each cell to improve steady-state precision.

From Fig. 16, it can be clearly seen that a basic FC is a PD controller, and from the increment expression of PI controller

$$\begin{aligned}\Delta u(k) &= K_p\left[(e(k) - e(k-1)) + \frac{1}{T_i}e(k)\right] \\ &= K_p\left[ce(k) + K_i e(k)\right]\end{aligned} \tag{22}$$

an important relation can be found, that is, the same input variables as that of the FC are used in (22). This makes it very natural and rational to embed NPI in each cell of the fuzzy con-

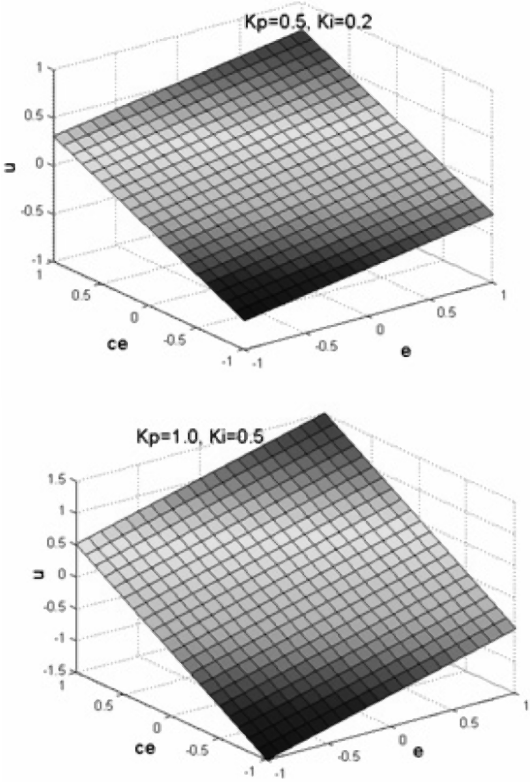

Fig. 18. Control surfaces of PI controller.

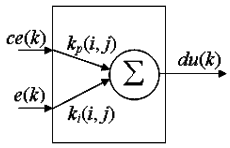

Fig. 19. Single neuron.

trol table. For a traditional PI controller, its control surface is a spacial plane. Fig. 18 gives two control surfaces with different PI parameters. However, according to Table III, for the NPIFC, the control space is composed of 169 subspacial planes. Each subspacial plane can be changed with the parameter change of NPI. Therefore, they make up a nonlinear special surface in the three-dimension space based on the fuzzy control table.

The process and steps of designing NPIFC are given as follows.

Step 1) Constructing NPI. The controller structure should express (22). Fig. 19 gives the structure of a NPI, where i and j denote the row label and column label of Table III. Notation $\sum$ denotes the summing operation, that is

$$du(k) = k_p(i,j) \cdot ce(k) + k_i(i,j) \cdot e(k). \tag{23}$$

Step 2) Constructing algorithm of adjusting weight coefficients. In (22), the NPI parameters $k_p(i,j)$ and $k_i(i,j)$ are expressed using two weight coefficients. They can be updated online. Because each NPI manages a small subpartition, convergence of learning algorithm becomes easier than neural networks. Thus, a least square formula and a gradient descend method are used as optimization index and optimization algorithm in this paper. The iterative formulas of $k_p(i,j)$ and $k_i(i,j)$ can be derived as follows:

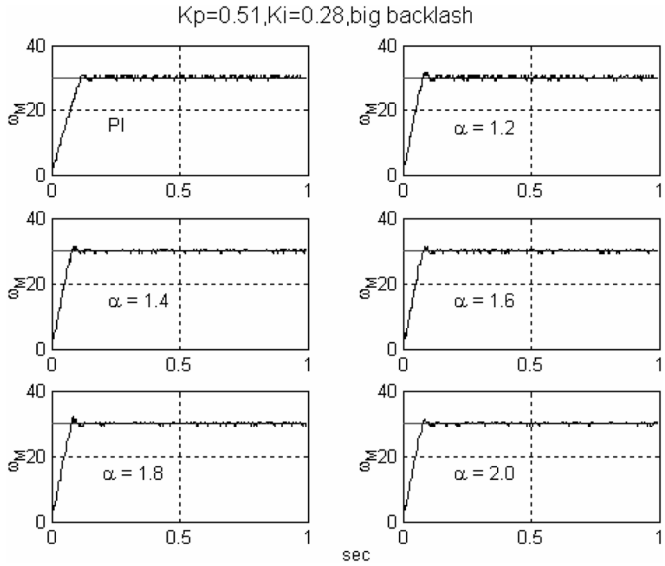

Fig. 20. Response with big backlash.

$$\Delta k_p(k) = \eta_p e(k) sgn\left(\frac{\partial y(k)}{\partial u(k)}\right) ce(k) + \nu k_p(k-1) \tag{24}$$

$$\Delta k_i(k) = \eta_i e(k)^2 sgn\left(\frac{\partial y(k)}{\partial u(k)}\right) + \nu k_i(k-1) \tag{25}$$

where η_p and η_i are the learning ratio of $k_p(i,j)$ and $k_i(i,j)$, ν is the inertial coefficient.

Step 3) Assigning initial weight values. The control output value $du(i,j)$ of the control table can be utilized to set the initial weights of neural cell, and assignment formula is derived from

$$k_{p\_ini}(i,j) \times ce_m + k_{i\_ini}(i,j) \times e_m = du(i,j) \tag{26}$$

and is rewritten as

$$k_{p\_ini}(i,j) k_{i\_ini}(i,j) = \frac{du(i,j)}{e_m + ce_m}. \tag{27}$$

Alternatively, some random numbers can be used as initial weight values.

Step 4) Selecting switching value between FC and NPIFC. The switching value is decided by selecting proper error and change-in-error. For instance, these cells outlined in Table III form an area. When error and change-in-error move into this area, NPI controller is switched.

Step 5) Updating the fuzzy control table. These cells outlined in Table III will be update by

$$du_{\text{new}}(i,j) = k_p(i,j) \times ce(k) + k_i(i,j) \times e(k). \tag{28}$$

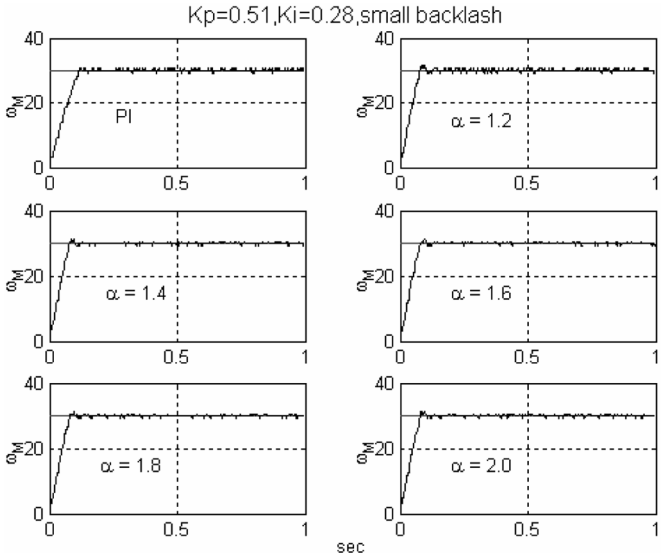

Fig. 21. Response with small backlash.

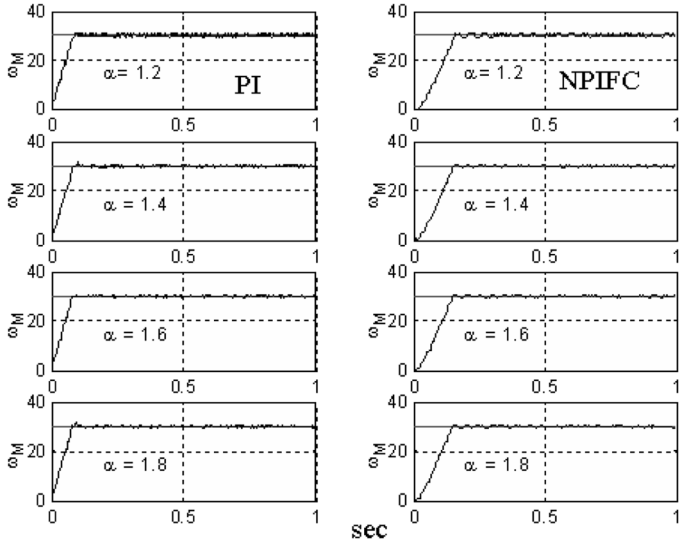

Fig. 22. Responses of using PI and NPIFC.

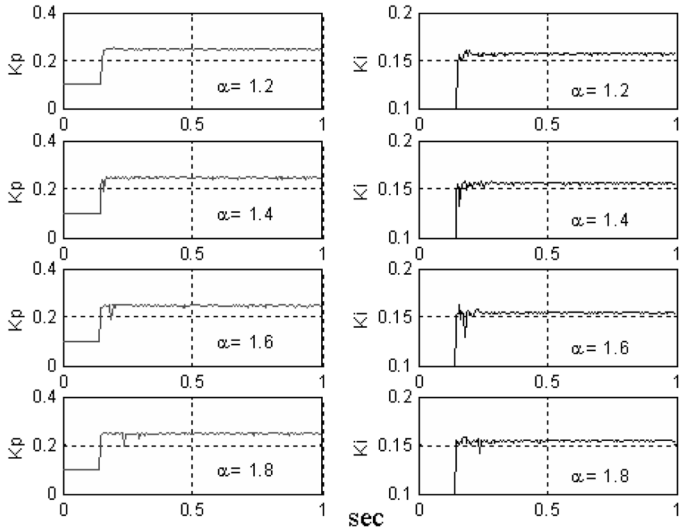

Fig. 23. Parameter self-tuning curves.

From the above design, it is can be seen that this NPIFC has some features.

1) Because only these NPI selected in the control table are able to be modified, a suitable compromise can be realized between the robust property of FC and higher steady-state precision of the PI controller.
2) Because PI is based on a single neuron, the controller has simplest iterative algorithm as well as learning performance.
3) Because the controller is composed of 169 NPI with different parameters, the controller becomes a distributing parameter controller with adaptive function. For each control step, control operation comes from a simple linear controller. But for the whole control process, control action is generated from a complex nonlinear controller.

IV. Experimental Verifications of Vibration Suppression

In the experimental verifications, three groups of vibration suppression experiments were conducted on the experimental system, as shown in Fig. 1. System parameters are given in Table I. In addition, the backlash of experimental system can be adjusted with a knob. Here, three kinds of cases, biggest, middle, and smallest backlashes were considered. In the following experiments, the sampling period was 0.001 s and the target angular speed ω_M of driver was 30 rad/s.

- Group 1: Biggest backlash was set. First, traditional PI controller was adopted to test control effect. Then, parameters of the PI controller, $Kp = 0.51$ and $Ki = 0.28$, were maintained, and FO-DOB was embedded into the inner loop. The $Q_\alpha(s)$-filter is approximated by (19) in the frequency bandwidth [100,10000]. The same test was done repeatedly when let fractional-order $\alpha = 1.2$, 1.4, 1.6, 1.8, 2.0, respectively.
- Group 2: Smallest backlash was set. The same process as Group 1 was carried out.
- Group 3: Middle backlash was set and FO-DOB was embedded into the inner loop. First, traditional PI controller was used with $Kp = 0.8$ and $Ki = 0.1$. Then, the NPIFC was used. Let fractional-order $\alpha = 1.2$, 1.4, 1.6, 1.8 and tested the control effect, respectively.

For experiments of Groups 1 and 2, related test curves are given in Figs. 20 and 21. From Figs. 20 and 21, it can be seen that when pure PI controller is used, vibration attenuation is not good no matter how the backlash is, biggest or smallest. In contrast, when FO-DOB is added in and $\alpha > 1.2$, the effect of vibration attenuation is better than the effect only using pure PI obviously. Thus, experiment results show that when FO-DOB is introduced, the system has better robust stability than if the PI controller is used alone, and it also can be found that the relative degree of $\alpha > 1.2$ should be selected in this system.

For the experiments of Group 3, Fig. 22 gives time response of using PI controller and NPIFC, respectively. Fig. 23 shows parameter self-tuning curves of the NPI. It can be found that

TABLE IV
ERRORS COMPARISON

error	α	PI	FC
Average of absolute error	1.2	0.381662	0.350781
	1.4	0.399857	0.331044
	1.6	0.452239	0.379055
	1.8	0.364514	0.390678
Relative Error (%)	1.2	0.012722	0.011693
	1.4	0.013329	0.011035
	1.6	0.015075	0.012635
	1.8	0.012150	0.013023

when time is about 0.14 s, NPI was switched. After that, through several times of self-tuning, Kp and Ki were maintained at 0.248 and 0.156, respectively. Table IV shows the error analysis of Fig. 22.

V. CONCLUSION

Fractional-order disturbance observer has attractive flexibility than the classical disturbance observer, because the introduction of fractional calculus makes universe of relative degree n_q of Q-filter expanded from integer domain to real-number domain. Therefore, the system has a more wide range to acquire a more suitable synthesis between robust stability and vibration suppression. The NPIFC makes use of properties of fuzzy control, neural control, and PI control synthetically, to realize vibration suppression effectively. The above design and experiments illustrate that this combination of FO-DOB and NPIFC can improve the performance of disturbance suppression and robustness of system.

REFERENCES

[1] M. Tomizuka, "Controller structure for robust high-speed/high-accuracy digital motion control," in *Proc. IEEE Int. Conf, Robot. Automat.*, San Diego, CA, 1995.

[2] T. Umeno and Y. Hori, "Robust speed control of dc servomotors using modern two degrees-of-freedom controller design," *IEEE Trans. Ind. Electron.*, vol. 38, no. 5, pp. 363–368, Oct. 1991.

[3] Y. Q. Chen, B. M. Vinagre, and I. Podlubny, "Fractional order disturbance observer for robust vibration suppression," *Nonlinear Dynamics*, vol. 38, pp. 355–367, 2004.

[4] C. J. Kempf and S. Kobayashi, "Disturbance observer and feedforward design for a high-speed direct-drive positioning table," *IEEE Trans. Control Syst. Technol.*, vol. 7, no. 5, pp. 513–526, Sep. 1999.

[5] T. Ohmae *et al.*, "A microprocessor-based motor speed regulator using FST response state observer for reduction of torsional vibration," *IEEE Trans. Ind. Applicat.*, vol. 23, pp. 863–871, 1987.

[6] M. Sugano *et al.*, "Torsional vibration suppression control by speed differentiation," in *Proc. IEE-Jpn. Tech. Meeting, SPC-*, 1990, pp. 90–109.

[7] H. Sugimoto, "Speed control of two inertia resonant system with integrator added observer," *Trans. IEE-Jpn*, vol. 111-D, no. 9, pp. 798–799, 1999.

[8] Y. Hori *et al.*, "Slow resonance ratio control for vibration suppression and disturbance rejection in torsional system," *IEEE Trans. Ind. Electron*, vol. 46, no. 1, pp. 162–168, Feb. 1999.

[9] J. K. Ji and S. K. Sul, "Kalman filter and LQ based speed controller for torsional vibration suppression in 2-mass motor drive system," *IEEE Trans. Ind. Electron*, vol. 42, no. 6, pp. 564–571, 1995.

[10] K. Kaneko *et al.*, "Accurate torque control for a geared dc motor based on acceleration controller," in *Proc. IEEE IECON*, 1992, vol. 2, pp. 309–315.

[11] F. Qiao, W. Duan, and C. J. Li, "Study of vibration suppression in the 2-mass main drive system of rolling mill," in *Proc. 7th CACSCUK*, Nottingham, U.K., 2001, pp. 205–212.

[12] Y. Q. Chen, B. M. Vinagre, and I. Podlubny, "On fractional order disturbance observer," in *Proc. DETC*, Chicago, IL, 2003, pp. 1–8.

[13] Y. Hori, "Vibration suppression and disturbance rejection control on torsional systems," in *Proc. IFAC Motion Control*, Munchen, 1995, pp. 41–50.

[14] J. K. Liu, *Advance PID Control and MATLAB Simulation*. Beijing, China: Publishing House of Electronics Industry, 2003.

[15] A. Oustaloup *et al.*, "Frequency-band complex noninteger differentiator: Characterization and synthesis," *IEEE Trans. Circuit Syst.-I: Fundamental Theory and Applications*, vol. 47, no. 1, pp. 25–39, Jan. 2000.

[16] L. X. Wang, "Fuzzy systems are universal approximators," in *Proc. 1st IEEE Conf. Fuzzy Syst.*, San Diego, CA, 1992, pp. 1163–1170.

Wen Li received the B.S. degree in industry automation and the M.S. degree in railway traction electrization and automation from Dalian Jiaotong University, Dalian, China, in 1982 and 1992, respectively, and the Eng.D. degree in control theory and control engineering from the Harbin Institute of Technology, Harbin, China.

Since 1982, she has been with the Department of Electrical Engineering, Dalian Jiaotong University, where, since 2001, she has been a Professor. She worked at the University of Tokyo, Tokyo, Japan, as a Visiting Researcher in 2005. Her research interests include intelligent control, fuzzy systems modeling, and control theory and its industrial application.

Prof. Li is a member of the China Railway Society.

Yoichi Hori (S'81–M'83–SM'00–F'05) received the B.S., M.S., and Ph.D. degrees in electrical engineering from the University of Tokyo, Tokyo, Japan, in 1978, 1980, and 1983, respectively.

In 1983, he joined the Department of Electrical Engineering, University of Tokyo, as a Research Associate. He later became an Assistant Professor, an Associate Professor, and in 2000 a Professor. In 2002, he moved to the Institute of Industrial Science, University of Tokyo, as a Professor in the Information and Electronics Division, Electrical Control System Engineering. During 1991–1992, he was a Visiting Researcher at the University of California, Berkeley (UCB). His research fields are control theory and its industrial application to motion control, mechatronics, robotics, electric vehicle, etc.

Dr. Hori is a member of the Institute of Electrical Engineers of Japan (IEE-Japan), Japan Society of Mechanical Engineers (JSME), the Society of Instrument and Control Engineers (SICE), the Robotic Society of Japan (RSJ), the Japan Society of Mechanical Engineers (JSME), and the Society of Automotive Engineers of Japan (SAEJ). He served as the Treasurer of the IEEE Japan Council and Tokyo Section during 2001–2002. He is now the Vice President of the IEE-Japan IAS.